THE JOURNAL OF BIOLOGICAL CHEMISTRY VOL. 290, NO. 6, pp. 3612–3621, February 6, 2015

The Olfactomedin Domain from Gliomedin Is a β-Propeller with Unique Structural Properties*

Received for publication, November 21, 2014, and in revised form, December 12, 2014 Published, JBC Papers in Press, December 17, 2014, DOI 10.1074/jbc.M114.627547

Huijong Han[‡§] **and Petri Kursula**[‡§¶1]

From the [‡]*Faculty of Biochemistry and Molecular Medicine and Biocenter Oulu, University of Oulu, 90014 Oulu, Finland, the* [§]*German Electron Synchrotron (DESY), 22607 Hamburg, Germany, and the* [¶]*Department of Biomedicine, University of Bergen, N-5020 Bergen, Norway*

Background: Gliomedin contains an olfactomedin (OLF) domain, for which structural information has been lacking.
Results: The crystal structure of the OLF domain from gliomedin was solved.
Conclusion: The OLF domain is a five-bladed β-propeller with broken symmetry.
Significance: The results provide a structural basis for gliomedin function and shed light on mutations in the human OLF family.

All members of the olfactomedin (OLF) family have a conserved extracellular OLF domain, for which a structure has not been available. We present here the crystal structure of the OLF domain from gliomedin. Gliomedin is a protein expressed by Schwann cells in peripheral nerves, important for the formation of the nodes of Ranvier. Gliomedin interacts with neuronal cell adhesion molecules, such as neurofascin, but the structural details of the interaction are not known. The structure of the OLF domain presents a five-bladed β-propeller fold with unusual geometric properties. The symmetry of the structure is not 5-fold, but rather reveals a twisted arrangement. The conserved top face of the gliomedin OLF domain is likely to be important for binding to neuronal ligands. Our results provide a structural basis for the functions of gliomedin in Schwann cells, enable the understanding of the role of the gliomedin OLF domain in autoimmune neuropathies, and unravel the locations of human disease-causing mutations in other OLF family members, including myocilin.

Rapid propagation of action potentials is important for the normal functioning of the nervous system. Myelin is a multilayered membrane that enables the fast saltatory conduction of nerve impulses along axons. Although myelin acts as an electric insulator, it also drives the localization and clustering of voltage-gated sodium (Na_v)[2] channels on the neuronal plasma membrane (1–3), a crucial feature for saltatory conduction whereby the nerve impulse "jumps" from one node of Ranvier to the next.

Gliomedin is a protein expressed by myelinating Schwann cells that is important for the formation of the nodes of Ranvier and clustering of Na_v channels on the axonal plasma membrane at the node (4–6). Gliomedin contains an extracellular olfactomedin (OLF) domain, which is able to induce channel clustering (7, 8). Gliomedin molecular ligands include neurofascin and NrCAM (neuronal cell adhesion molecule) (5, 9), and loss of neuronal neurofascin also results in depletion of gliomedin from the nodes of Ranvier (10). Gliomedin is a type II transmembrane protein, and in addition to its C-terminal OLF domain, it harbors an extracellular collagen-like domain, which mediates gliomedin trimerization (8). Gliomedin homologs have also been identified in invertebrates (11). *In vivo*, gliomedin is processed proteolytically, and the extracellular OLF domain can be released either with or without the collagen domain (7, 8). The OLF domain is also glycosylated (8), although the exact sites and nature of glycosylation have not been determined.

The ~250-residue OLF domain was first discovered in the early 1990s (12). All members of the OLF protein family contain an extracellular OLF domain (13). OLF domains are mediators of extracellular protein interactions, and they play roles in diverse processes, such as nervous system development, intercellular adhesion, and cell cycle regulation (14). Although the structure of the OLF domain has remained unknown, it can be predicted to consist largely of β-structure. The OLF domain of myocilin was suggested to form a six-bladed β-propeller structure (15), but no experimental data have backed up this prediction.

Due to its direct disease linkage, the most widely studied OLF family member is myocilin, mutations in which cause primary open-angle glaucoma in humans (16–18). Myocilin is also involved in myelination, especially in the optic nerve (19–22). The sequence identity between the OLF domains of gliomedin and myocilin is only 22%, however, suggesting that they do not carry out overlapping functions. An interaction between gliomedin and myocilin has also been reported (20).

We determined the high-resolution crystal structure of the OLF domain from gliomedin. The structure presents an unusual β-propeller fold, and it can be used both to understand

* This work was supported by European Community Seventh Framework Programme FP7/2007–2013 under BioStruct-X Grant 283570 and by grants from the Academy of Finland, the Sigrid Jusélius Foundation, the Emil Aaltonen Foundation, and the Research and Science Foundation of the City of Hamburg.

The atomic coordinates and structure factors (codes 4D77 and 4D7C) have been deposited in the Protein Data Bank (http://wwpdb.org/).

[1] To whom correspondence should be addressed: Dept. of Biomedicine, University of Bergen, Jonas Lies vei 91, N-5020 Bergen, Norway. Tel.: 47-5558-6438; E-mail: petri.kursula@biomed.uib.no.

[2] The abbreviations used are: Na_v, voltage-gated sodium; OLF, olfactomedin; SAXS, small-angle x-ray scattering; CHES, 2-(cyclohexylamino)ethanesulfonic acid.

the involvement of gliomedin in neurological development and disease and to obtain information on disease-related mutations in related OLF family members, such as myocilin.

EXPERIMENTAL PROCEDURES

Protein Expression and Purification—The OLF domain of rat gliomedin (residues 260–543; sequence numbering includes the signal sequence) was recombinantly expressed in baculovirus-infected insect cells (23). Purification consisted of nickel-nitrilotriacetic acid affinity chromatography, His tag cleavage using tobacco etch virus protease, and size-exclusion chromatography (23). The OLF domain was predicted by sequence analysis to lie at the very C terminus, whereas the N-terminal boundary of the domain was difficult to pinpoint. The domain selected for expression and structural studies ranged from the end of the collagen-like domain close to the C terminus. This construct provided a good yield of crystallizable recombinant protein.

Biophysical Characterization—CD spectroscopy was used to confirm the folding state of the purified gliomedin OLF domain. Spectra were measured on an Applied Photophysics Chirascan-plus instrument at +20 °C in a buffer containing 1.8 mM Tris (pH 7.5) and 7 mM NaCl. The protein concentration was 0.5 mg/ml, and the cuvette path length was 0.5 mm.

Synchrotron small-angle x-ray scattering (SAXS) data were obtained on the SWING beamline at the SOLEIL Synchrotron (Paris, France). The gliomedin OLF domain (6 mg/ml) was injected onto an Agilent SEC-3 size-exclusion column using an Agilent HPLC system and eluted with 0.1 M Tris (pH 7.5) and 400 mM NaCl. The eluate was directed to the SAXS flow-through capillary cell, and scattering data were collected online. Frames corresponding to the main peak were selected and averaged using FoxTrot. Following data processing, further analyses were performed with the ATSAS package (24). GASBOR (25) was used for *ab initio* model building. CORAL (24) was used in conjunction with the crystal structure to build the fragments not visible in the crystal.

Crystallization and Data Collection—Highly concentrated pure gliomedin OLF domain (23 mg/ml) in 50 mM Tris (pH 7.5) and 100 mM NaCl was used for crystallization. After 3 days of incubation at 293 K, crystals were observed in 0.1 M CHES (pH 9.5) containing 20% PEG 8000. The crystals were picked up in a LithoLoop (Molecular Dimensions), briefly immersed in mother liquor supplemented with 20% 2-methyl-2,4-pentanediol, and flash-cooled in liquid nitrogen. Diffraction data for these orthorhombic native crystals were collected on the ID23-1 beamline at the European Synchrotron Radiation Facility (ESRF, Grenoble, France). Data collection for the monoclinic crystal form was reported previously (23).

For experimental phasing, a large number of derivatives using heavy metal compounds and halides were prepared and tested. Eventually, a strong anomalous signal was observed from a single crystal soaked in K_2PtCl_4. Single-wavelength anomalous dispersion data were collected on beamline 14.1 at the Helmholtz-Zentrum Berlin/Berliner Elektronen-Speicherring Gesellschaft für Synchrotronstrahlung (HZB/BESSY, Berlin, Germany). All diffraction data were processed with XDS (26).

Structure Solution and Refinement—The structure was solved using the single-wavelength anomalous dispersion protocol of Auto-Rickshaw, the European Molecular Biology Laboratory (EMBL) Hamburg automated crystal structure determination platform (27). The input diffraction data were prepared and converted for use in Auto-Rickshaw using programs of the CCP4 suite (28).

Estimated substructure structure factor amplitude values were calculated using SHELXC (29). Based on an initial analysis of the data, the maximum resolution for substructure determination and initial phase calculation was set to 2.61 Å. Heavy atoms were found with SHELXD (30), and the correct hand for the substructure was determined using ABS (31) and SHELXE (32). Initial phases were calculated after density modification using SHELXE (32). The 2-fold non-crystallographic symmetry operator was found using RESOLVE (33). Density modification, phase extension, and non-crystallographic symmetry averaging were performed with dm (34). Two chains of 242 residues each were thereafter automatically built using ARP/wARP (35, 36).

The automatic pipeline further refined this partial model to 2.0 Å resolution with the platinum derivative data using CNS (37), Refmac5 (38), and PHENIX (39). The partially refined structure was then used as a template for molecular replacement against a native high-resolution data set in a different space group. The structure was further refined using PHENIX and manually built using Coot (40). The final coordinates and original structure factors were deposited in the Protein Data Bank with codes 4D77 (orthorhombic) and 4D7C (monoclinic).

Homology Searches and Structure Analysis—Homologous structures were searched using PDBeFold (41) and SALAMI (42). For structure analysis and visualization, the programs PyMOL, UCSF Chimera (43), WEBnm@ (44), CCP4mg (45), and ConSurf (46) were used. A homology model for the myocilin OLF domain was constructed based on sequence alignment between myocilin and gliomedin using SWISS-MODEL (47).

RESULTS

Crystal Structure of the Gliomedin OLF Domain—Gliomedin contains an N-terminal transmembrane domain, a collagen-like segment, and a C-terminal OLF domain (Fig. 1*A*). The structure of the rat gliomedin OLF domain was solved by single-wavelength anomalous dispersion phasing using a crystal derivatized with platinum, and the structure was refined to 1.49 Å resolution using native data (Table 1). The OLF domain structure is composed of a five-bladed β-propeller (Fig. 1*B*), and each blade contains four β-strands (strands a–d). The overall dimensions of the OLF domain are ~30 × 40 × 40 Å. Like other β-propellers, the OLF domain is disc-shaped. The propeller circle is closed by insertion of the first N-terminal β-strand into the framework of the last propeller blade (Fig. 1*B*), which is a common mechanism in β-propeller proteins, also termed Velcro closure (48). The structure also contains three short α-helices. The longest of these helices is located in a loop between β-strands c and d of blade 1. Interestingly, normal mode analysis of the structure suggests that this helix is highly mobile, and there may be significant motions between blades 1 and 5 (data not shown). In general terms, normal mode analysis allows the identification of potential low-frequency, large-amplitude,

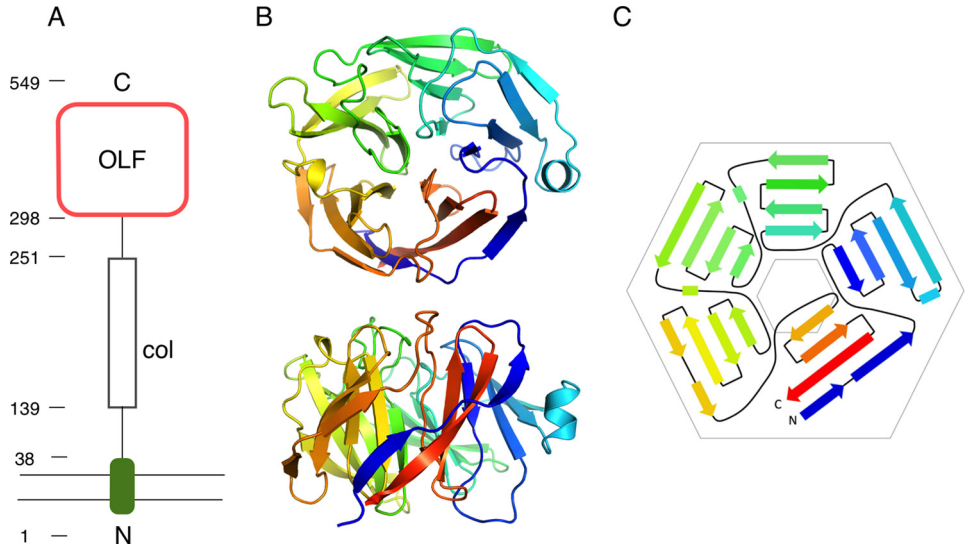

FIGURE 1. **Overall structure of the gliomedin OLF domain.** *A*, schematic drawing of full-length gliomedin, which has an OLF domain at its C terminus. Residue numbering for predicted domain boundaries is shown to the left. *col*, collagen-like domain. *B*, crystal structure of the C-terminal OLF domain from gliomedin, viewed from above (*upper*) and the side (*lower*). The N terminus (*blue*) closes the ring-like structure by providing a β-strand to the C-terminal blade. *C*, topology diagram for the OLF domain. The structure is a β-propeller with five blades, but blades 1–4 follow hexagonal symmetry.

TABLE 1

Crystallographic data collection and refinement

Pt-SAD, platinum-based single-wavelength anomalous dispersion.

	Data set		
	Pt-SAD	Native	Native 2
Data collection			
Beamline	14.1 (BESSY)	ID23-1 (ESRF)	ID23-2 (ESRF)
Wavelength (Å)	1.071	0.954	0.873
Unit cell parameters	$a = 45.5$, $b = 100.7$, $c = 59.3$ Å; $\beta = 90.05°$	$a = 45.8$, $b = 62.5$, $c = 88.3$ Å	$a = 37.6$, $b = 141.7$, $c = 46.0$ Å; $\beta = 110.6°$
Space group	$P2_1$	$P2_12_12_1$	$P2_1$
Resolution (Å)[a]	50-2.01 (2.06-2.01)	50-1.48 (1.52-1.48)	50-1.45 (1.49-1.45)
No. of reflections	63,785 (4753)	42,999 (3127)	78,451 (5723)
R_{merge} (%)	4.3 (32.0)	4.6 (193.2)	9.9 (101.7)
$\langle I/\sigma I \rangle$	10.4 (2.6)	18.3 (1.0)	8.4 (1.3)
Completeness (%)	90.4 (89.5)	99.9 (99.9)	98.7 (97.4)
Redundancy	1.5 (1.5)	6.5 (6.3)	3.7 (3.6)
$CC_{1/2}$ (%)[b]	99.7 (82.7)	100.0 (31.7)	99.7 (48.0)
Wilson *B* factor (Å^2)	37.0	31.4	20.6
Refinement			
R_{work}/R_{free} (%)		13.7/16.3	17.3/21.2
Root mean square deviation			
Bond lengths (Å)		0.007	0.015
Bond angles		1.2°	1.0°
MolProbity score (percentile)[c]		1.14 (98th)	1.32 (94th)
Ramachandran most favored (%)[c]		97.2	97.0
Ramachandran outliers (%)[c]		0.4	0.4
Average *B* factor (Å^2), protein, solvent		34.3/42.2	20.7/29.2
Protein chains/asymmetric unit	2	1	2
Protein Data Bank code		4D77	4D7C

[a] The values in parentheses refer to the highest resolution shell.
[b] $CC_{1/2}$ is the correlation coefficient between two random half-data sets (69).
[c] Validation was carried out using MolProbity (70).

concerted motions in a protein structure. A schematic representation of the OLF domain topology is shown in Fig. 1*C*.

The common fold of a β-propeller structure contains 4–10 antiparallel four-stranded β-sheets (49). Upon close inspection, the OLF domain five-bladed fold lacks a regular 5-fold symmetry and appears twisted. Indeed, blades 1–4 are actually arranged according to a hexagonal setting (Fig. 1*C*). The remaining blade 5, which contains both the N and C termini, actually takes up the space that would be filled by two blades in a six-bladed β-propeller. This arrangement is certainly unexpected and unusual, and it distinguishes the OLF domain from both five- and six-bladed β-propellers, also explaining difficulties in correctly predicting the OLF domain structure.

Structural homology searches using different algorithms with the gliomedin OLF domain produced rather poor hits to β-propeller structures, and both five- and six-bladed structures were detected. However, when only blades 1–4 were used in searches, better fits were obtained toward six-bladed structures. This further highlights the loss of 5-fold symmetry in the OLF domain and confirms the 6-fold symmetry obeyed by the first four blades. Superpositions on symmetric five- and six-bladed structures further proved this arrangement (Fig. 2).

Surface Properties—To obtain an insight into possible functionally important sites on the gliomedin OLF domain surface, we analyzed its surface properties. The electrostatic surface of the gliomedin OLF domain shows a high positive charge on the

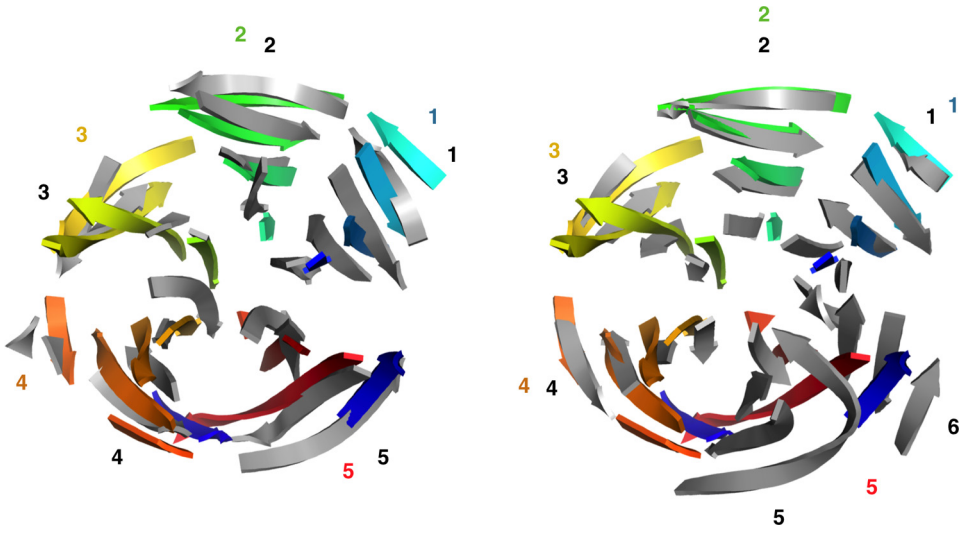

FIGURE 2. **Comparison of gliomedin with other β-propellers.** Superposition on a canonically symmetric five-bladed β-propeller structure (71) indicates poor overlap of the β-sheet blades (*left*). Superposition based on blades 1–4 on a six-bladed structure (72) gives a much better fit for these blades (*right*), which are organized in hexagonal symmetry. Blade 5 overlaps with blades 5 and 6 of the 6-fold structure. For clarity, only β-strands from the respective structures are shown. In both panels, the gliomedin OLF domain is colored, and the corresponding reference structures are shown in *gray*.

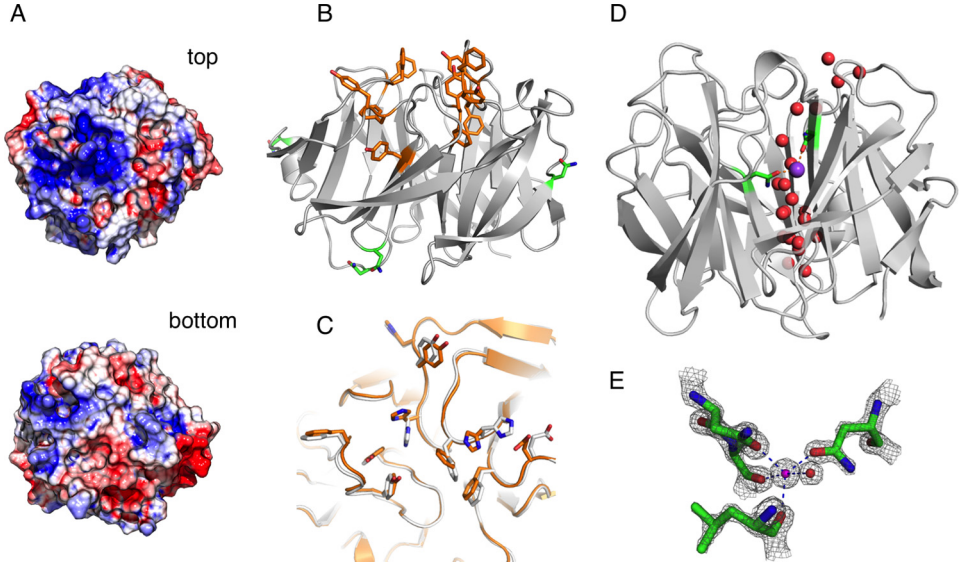

FIGURE 3. **Structural details of the gliomedin OLF domain.** *A*, electrostatic surfaces of the top and bottom faces. *B*, aromatic residues (*orange*) are clustered on the top face of the OLF domain, and the glycosylation sites (*green*) are on the side. *C*, different conformations of the aromatic surface in the two crystal forms. *D*, the solvent cavity inside the gliomedin OLF domain contains a number of water molecules and a sodium ion (*magenta*). *E*, electron density of the sodium-binding site. Shown is the $2F_o - F_c$ density contoured at 3σ. All coordination distances (*dashed lines*) are between 2.27 and 2.44 Å.

top face, whereas the bottom is more neutral or even negatively charged (Fig. 3*A*). The positive charge may be important in attracting binding partners of gliomedin.

The distribution of aromatic residues on the surface of the OLF domain (Fig. 3*B*) indicates a possible surface for protein interaction with several aromatic rings. For example, carbohydrate ligands would be candidates for interaction with the OLF domain.

The OLF domain structure was also refined in a monoclinic crystal form, and an apparent concerted movement of large side chains at the top face between the two crystal forms was observed (Fig. 3*C*). This indicates some flexibility in the structure, which could be important for interactions. A plasticity of the aromatic surface could allow binding of diverse protein and/or carbohydrate ligands.

Gliomedin is known to be glycosylated on its OLF domain (8), and a total of four possible *N*-glycosylation sites can be predicted to lie within the domain. The crystal structure indicates that all these possible sites of glycosylation lie on the surface. Remarkably, all the sites are on the "side" of the OLF domain, keeping the top face accessible (Fig. 3*B*).

Solvent Cavity and Cation-binding Site—In general, β-propellers have a central cavity, where, for example, enzymatic active sites can reside. The cavity or channel size increases as the number of blades gets higher (49). Gliomedin has a much smaller central cavity due to the disrupted symmetry. Furthermore, the top of this cavity is closed by a long loop (connecting strands 2d–3a), and it contains a number of water molecules and a bound cation (Fig. 3*D*).

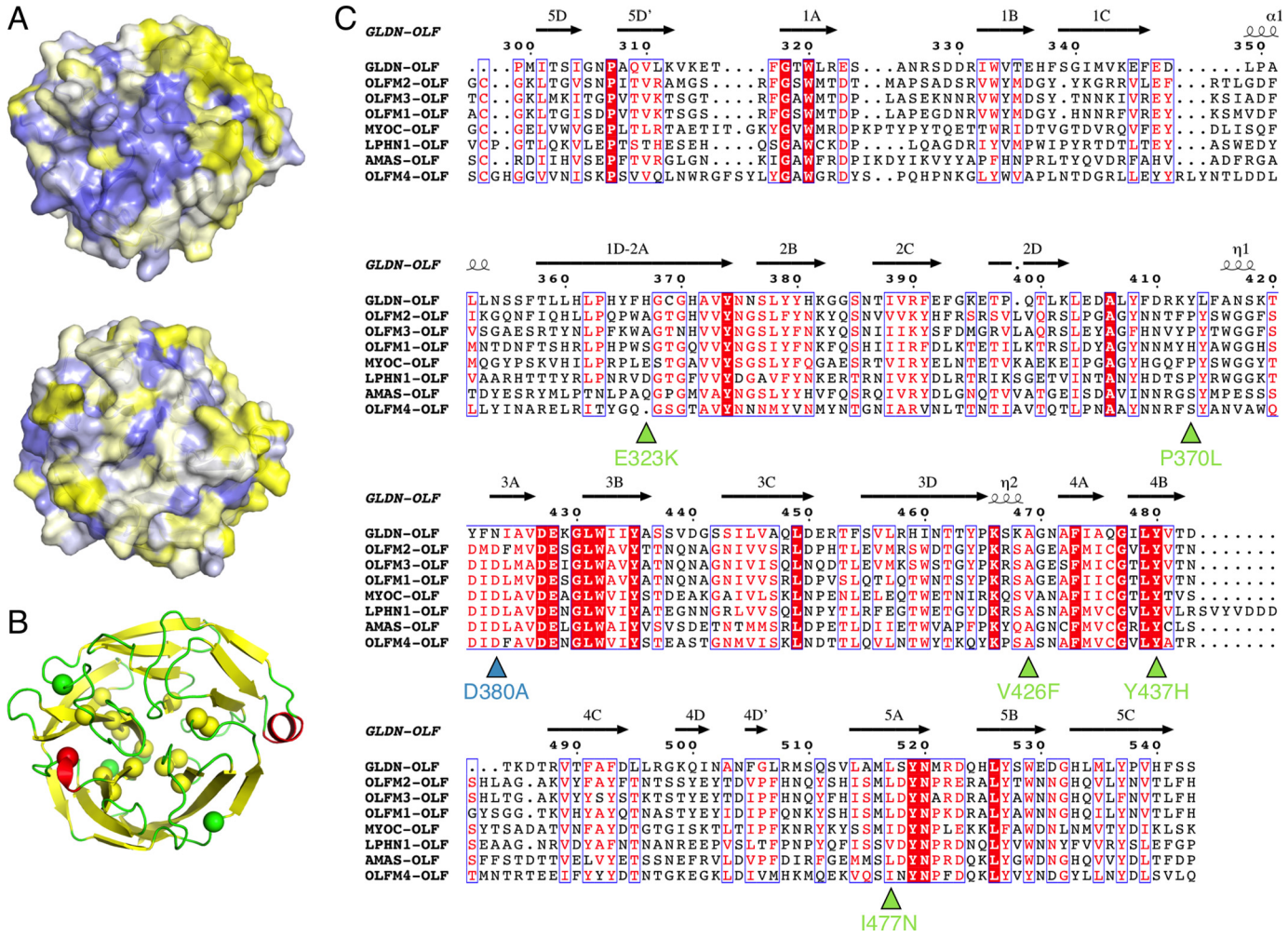

FIGURE 4. **Sequence conservation of OLF domains at the structural level.** *A*, conservation in gliomedins from different species. *Blue* indicates high and *yellow* indicates poor conservation. The top surface (*upper*) is highly conserved across species, whereas the bottom surface (*lower*) is poorly conserved. *B*, top view of the gliomedin OLF domain. Residues that are fully conserved in OLF domains are shown as *spheres*. *C*, sequence alignment of rat gliomedin (*GLDN*), sea urchin amassin (*AMAS*), and various human OLF domains (*OLFM*, olfactomedin; *MYOC*, myocilin; *LPHN*, latrophilin). The fully conserved residues are highlighted in *B*. The *triangles* below the alignment highlight some of the most severe mutations in human myocilin (*green*) and the location of the calcium-coordinating mutation site D380A (*blue*).

A positively charged ion is present inside the gliomedin OLF structure, on the side of the water-filled cavity. The ion is well defined in electron density and coordinated by five oxygen atoms at distances of ~2.30 Å (Fig. 3*E*). Also taking into account the buffer composition in crystallization, this ion could be confidently built as Na^+. The ion was also validated by the WASP (50) and CheckMyMetal (51) servers, and clearly the best scores were obtained for the presence of Na^+. In particular, the Na^+-specific valence value of 1.1 calculated by WASP clearly indicates bound Na^+ (50). The side chains of Asn-423 and Asn-471 are involved in the coordination, as are the backbone carbonyl groups of Ala-472 and Leu-517 and one water molecule. Notably, Asn-423 corresponds to Asp-380 in myocilin. Myocilin was shown to bind and be stabilized by calcium (52), and the D380A mutation abolished calcium binding, as well as the calcium-induced increase in protein stability. This mutation is also a disease-causing variant in myocilin (see below for more discussion on myocilin mutations).

Conservation in Gliomedin from Different Species—To get a better idea of putative functionally important parts of the OLF domain structure, sequences of gliomedin from different species were compared with regard to sequence conservation. In general, the least conserved regions include the outermost β-strands in the blades. On the other hand, in addition to the protein core, residues on the top surface are highly conserved (Fig. 4*A*) and hence most likely involved in gliomedin function *in vivo*. This conservation coincides with the positive electrostatic potential and the location of the clusters of aromatic residues on the surface. The bottom face of the OLF domain is poorly conserved.

In addition to gliomedins, conservation was further checked for different representative OLF domain sequences (Fig. 4, *B* and *C*). Based on this analysis, 20 fully conserved residues were identified on OLF domains, of which three are glycine and seven are aromatic. It is obvious that these conserved residues are important for the unique structural aspects of the OLF domain fold due to their localization inside the fold. The top face of the OLF domain has none of these conserved sites, which is an indication of different binding preferences of OLF family proteins for their respective ligands.

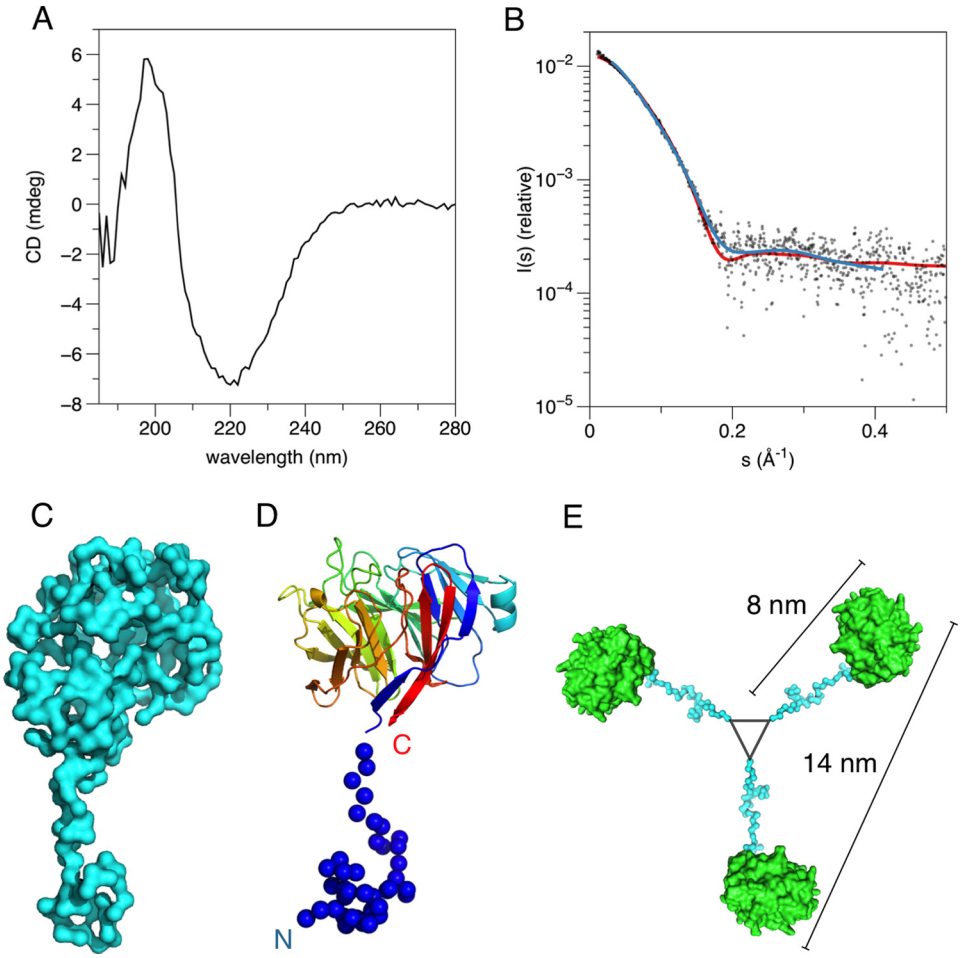

FIGURE 5. **Solution characterization of the gliomedin OLF domain.** *A*, the CD spectrum indicates a structure consisting mainly of β-sheet. *mdeg*, millidegrees. *B*, raw x-ray scattering data from the gliomedin OLF domain (*gray*) superimposed with fits from modeling with GASBOR (*blue*) and CORAL (*red*). *C*, *ab initio* modeling by GASBOR indicates an extended tail. *D*, CORAL building of parts missing in the crystal structure (*spheres*). *E*, based on the CORAL model, a trimer was constructed. The *triangle* in the middle represents the C-terminal end of the collagen triple helix of gliomedin. The dimensions of a monomeric and trimeric OLF domain are shown.

The OLF Domain Is a Monomer Folded into β-Structure in Solution—Gliomedin contains a collagen-like domain N-terminal to its OLF domain. In line with this, EM imaging has shown that gliomedin forms trimers through its collagen-like domain, such that the three OLF domains lie rather close to each other in space (8). To validate the crystal structure, which gives no indications of specific oligomerization, we characterized the OLF domain in solution.

Correct folding of the gliomedin OLF domain in solution was proven by CD spectroscopy, which shows clear hallmarks of β-structure (Fig. 5*A*). We further characterized the domain in solution using SAXS, and it behaves like a monomer (Fig. 5*B*). The SAXS data indicate a radius of gyration (R_g) of 2.4 nm and a maximum dimension (D_{max}) of 9 nm. These values are larger than those calculated (53) from the crystal structure (R_g = 1.7 nm, D_{max} = 5.3 nm), which is most likely caused by the N terminus, which is not observed in the crystal structure. The molecular mass, based on the excluded volume of the *ab initio* model, is 36 kDa, which is very close to that expected for a monomer (32.4 kDa). In three-dimensional modeling, good fits were obtained when the N terminus was implicitly modeled (Fig. 5, *B–D*). Also the OLF domain of myocilin has been characterized as a monomer *in vitro* (54, 55).

Structural modeling based on solution scattering data indicates that the construct used in our studies includes an extension to the OLF domain; this most likely represents the disordered N terminus of the protein (Fig. 5, *C* and *D*). Although the OLF domain is sufficient to induce Na_v channel clustering, this process requires a pre-clustering of OLF domains (7, 8). Considering the fact that the disordered N terminus of our construct essentially lies at the end of the collagen-like trimerization domain, based on the SAXS model, we calculated the expected dimensions of the C-terminal OLF domain assembly in full-length gliomedin. Assuming the collagen-like domain indeed forms a triple helix, the interaction (top) surfaces of the OLF domains cannot be farther apart from each other than 14 nm (Fig. 5*E*). Of course, it is possible that they actually are closer to one another in the trimeric molecule.

Comparison with Other OLF Family Members—Within the OLF family, by far the largest body of research has been carried out on myocilin, which is understandable based on its direct involvement in human disease. Dozens of myocilin mutations in glaucoma patients have been described, and the vast majority of these map to the OLF domain (14), highlighting the crucial role of this domain in the physiological function of myocilin.

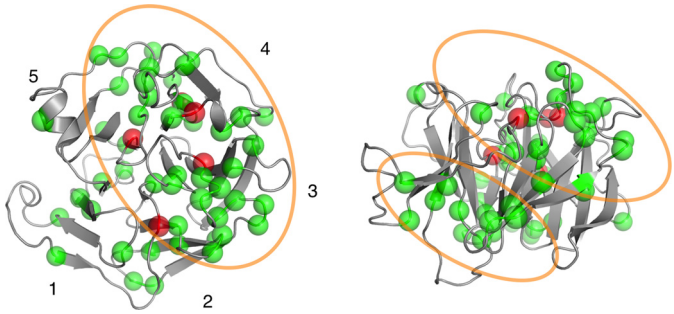

FIGURE 6. **Analysis of glaucoma mutations in the myocilin OLF domain.** Top (*left*) and side (*right*) views are shown to highlight the three-dimensional clustering of known mutations based on a homology model. The Cα atoms of affected residues are shown as *spheres*. Mutations described as severe (14) are shown in *red*; all other mutations are shown in *green*. The side view indicates very few mutations in the secondary structure elements. The *orange ellipsoids* highlight mutation clustering in the two views.

Using the gliomedin OLF domain crystal structure, a homology model was made for myocilin, which allowed mapping of the OLF domain glaucoma mutations onto the three-dimensional structure (Fig. 6). A number of observations on these mutations can be made. The first striking observation is that despite the β-propeller fold and reports on misfolding and/or abnormal processing of myocilin mutants (56–60), very few of the mutations are actually located in the β-strands; most of them affect loops between the strands. Analysis of mutation location in three-dimensional space further indicates hot-spot regions with highly concentrated mutations; this concerns especially the top face of blades 2–4 and, to some extent, the bottom side of blades 1 and 5 (Fig. 6). The locations of some of the most severe mutations (14) are discussed below.

DISCUSSION

OLF domain proteins are known to play essential roles in development and cell differentiation in both vertebrates and invertebrates; however, their functions are only partially known at the moment, and their high-resolution structures have remained unknown. We have presented the first crystal structure of an OLF domain, which in gliomedin is crucial for correct formation of the nodes of Ranvier in myelinated peripheral nerves. At a more general level, the structure can be used both to understand OLF domain function in different OLF family proteins and to predict and analyze the molecular effects of human disease-causing mutations affecting OLF domains.

In vertebrates, gliomedin is important for the clustering of Na_v channels at the nodes of Ranvier (61), a process that is a prerequisite for saltatory propagation of the action potential along axons. On the other hand, the gliomedin homolog *unc-122* in *Caenorhabditis elegans* is involved in neuromuscular signaling (11). Interestingly, the Na_v channel-clustering function of gliomedin can also be carried out by the isolated OLF domain (7, 8) as long as the OLF domain has been pre-clustered. Hence, the OLF domain crystal structure presented here directly represents the functional unit of gliomedin in the development of the nodes of Ranvier in the nervous system. Whether the clustering of three OLF domains together by the collagen triple helix is enough for this function or if larger scale aggregates are required *in vivo* is currently unclear.

A high-resolution structural study including the collagen-like domain N-terminal to the OLF domain would clarify how the three OLF domains are arranged in a gliomedin trimer. EM imaging provided a low-resolution view of this arrangement (8), in which the three OLF domains are close to each other in space, but not bound to each other. This fits our SAXS data and the model of a trimeric arrangement of monomeric OLF domains (Fig. 5*E*). In general, oligomerization via neighboring domains or disulfide bridges is a general feature of OLF domains; for example, myocilin has a coiled-coil dimerization domain instead of the collagen-like domain of gliomedin. Oligomerization of OLF domains through these adjacent regions thus appears to be crucial for their biological activity.

Gliomedin is known to bind to fibronectin type III-like domains of neurofascin and NrCAM (9). These domains contain locally concentrated, negatively charged residues, which could provide a binding site for the positively charged top face of the gliomedin OLF domain. However, the precise binding mode will remain unclear until structural information becomes available for such protein-protein complexes.

Five-bladed β-propeller structures are most often carbohydrate-binding proteins and/or enzymes (49). For gliomedin, apart from its interactions with neurofascin and NrCAM (5), few functional details are known at the molecular level. No enzymatic activity has been reported for OLF domains, and gliomedin is unlikely to harbor one.

Like many other myelin proteins, gliomedin is a target for autoantibodies in peripheral neuropathies (62–64), with implications for multifocal motor neuropathy, chronic inflammatory demyelinating polyneuropathy, and Guillain-Barré syndrome. The exact autoimmune epitopes on gliomedin are not yet known. The crystal structure of the OLF domain will now enable the identification of such epitopes to understand the effects of autoimmune attack on the nodes of Ranvier and the myelin sheath.

Myocilin is by far the best characterized OLF domain-containing protein; however, no published data exist on its three-dimensional structure. The gliomedin OLF domain structure enables us to understand the locations and effects of the plethora of human myocilin mutations causing glaucoma. In three-dimensional space, the human myocilin mutations clearly cluster in defined regions and are largely absent from the secondary structure elements (Fig. 6). This is surprising, as glaucoma mutations in general have been assumed to cause misfolding or abnormal processing of myocilin (56–60). The loops are apparently important for correct OLF domain folding.

A calcium-binding site was reported in myocilin, and it was suggested to involve Asp-380 (52). The glaucoma-causing mutation D380A has been intensively studied with regard to the loss of Ca^{2+}-binding affinity upon mutation (52). In the gliomedin structure, we detected a bound cation (most likely sodium) that is coordinated by Asn-423, corresponding in sequence to Asp-380 in myocilin (Figs. 3*E* and 4*C*). Thus, Asp-380 in myocilin is most likely located in a similar cavity and possibly chelates a calcium ion that stabilizes the structure. In all other OLF domains apart from gliomedin, this Asp is conserved (Fig. 4*C*), and calcium binding may be a general feature of the OLF domain, with the exception of gliomedin. Interest-

ingly, calcium is also required for the massive intercellular clotting involving the sea urchin OLF protein amassin (65, 66); it is not known, however, if this reflects a requirement of calcium binding for a functional amassin OLF domain. The second metal-coordinating side chain of gliomedin (Asn-471) is conserved in myocilin as Asn-428. We believe that the sodium-binding site observed in the gliomedin crystal structure spatially corresponds to the calcium-binding site of myocilin. Taking into account that the extracellular Na^+ concentration is expected to be higher than that of our buffers, it is likely that the site in gliomedin is also occupied by Na^+ *in vivo*. Furthermore, it is interesting to note that gliomedin is localized close to the nodes of Ranvier, at which Na^+ will rush into the axon when a nerve impulse passes, and that it is involved in the clustering of Na_v channels. Previously, Ca^{2+} binding by myocilin was reported to increase the stability of the OLF domain (52), and the binding of metals could clearly be a common mechanism to increase OLF domain stability. The functional relevance of metal binding by OLF domains clearly requires further study.

The residues corresponding to the myocilin mutations P370L and C433R (responsible for severe glaucoma phenotypes) are located on the loops between β-strands 2d and 3a and between β-strands 4a and 4b, respectively. These residues and the conformation of the loops are probably critical to forming and maintaining a stable β-propeller structure. Furthermore, Cys-433 has been suggested to form a disulfide bridge with Cys-245 in myocilin (67); in gliomedin, such a disulfide is missing. Cys-433 is conserved in all other OLF domains apart from gliomedin. Considering the myocilin homology model, Cys-433 is in close contact with Gly-246, which is the N-terminal residue of the homology model. Thus, Cys-245 would be at a perfect position to form a disulfide bond with Cys-433, and this linkage can be expected to stabilize the assembly of the myocilin OLF domain.

Another human glaucoma mutation is Y437H, which also can induce disease when injected into mice (68). The corresponding residue in gliomedin (Tyr-480) lies in the middle of β-strand 4b, surrounded by many hydrophobic residues. This indicates that Tyr-480 in gliomedin, which indeed is conserved in all OLF domains (Fig. 4*C*), may be a key residue to stabilize the β-propeller structure.

Of the 20 glycine residues in the myocilin OLF domain, a total of eight have been listed as glaucoma mutation sites (14). Essentially all these residues are located in loops between β-strands in the propeller blades. It is likely that their flexibility and their ability to support tight turns are of overall importance during the correct folding of the myocilin OLF domain. It is also logical to assume that glycine residues in the loops are involved in the folding of other OLF family members.

To conclude, we have presented the crystal structure of the OLF domain from gliomedin, which forms a twisted five-bladed β-propeller. The high-resolution OLF domain structure is an important step toward understanding the functions and mechanisms of OLF domains. It is likely that the tertiary structures of other OLF domains are highly similar to that of gliomedin. Hence, the OLF domain is a unique β-propeller, and OLF-containing proteins can be added to the list of β-propeller proteins involved in human development and disease.

Acknowledgements—We are grateful for synchrotron beam time and excellent support at BESSY, ESRF, and SOLEIL.

REFERENCES

1. Dugandzija-Novaković, S., Koszowski, A. G., Levinson, S. R., and Shrager, P. (1995) Clustering of Na^+ channels and node of Ranvier formation in remyelinating axons. *J. Neurosci.* **15,** 492–503
2. Kaplan, M. R., Meyer-Franke, A., Lambert, S., Bennett, V., Duncan, I. D., Levinson, S. R., and Barres, B. A. (1997) Induction of sodium channel clustering by oligodendrocytes. *Nature* **386,** 724–728
3. Vabnick, I., Novaković, S. D., Levinson, S. R., Schachner, M., and Shrager, P. (1996) The clustering of axonal sodium channels during development of the peripheral nervous system. *J. Neurosci.* **16,** 4914–4922
4. Occhi, S., Zambroni, D., Del Carro, U., Amadio, S., Sirkowski, E. E., Scherer, S. S., Campbell, K. P., Moore, S. A., Chen, Z. L., Strickland, S., Di Muzio, A., Uncini, A., Wrabetz, L., and Feltri, M. L. (2005) Both laminin and Schwann cell dystroglycan are necessary for proper clustering of sodium channels at nodes of Ranvier. *J. Neurosci.* **25,** 9418–9427
5. Eshed, Y., Feinberg, K., Poliak, S., Sabanay, H., Sarig-Nadir, O., Spiegel, I., Bermingham, J. R., Jr., and Peles, E. (2005) Gliomedin mediates Schwann cell-axon interaction and the molecular assembly of the nodes of Ranvier. *Neuron* **47,** 215–229
6. Amor, V., Feinberg, K., Eshed-Eisenbach, Y., Vainshtein, A., Frechter, S., Grumet, M., Rosenbluth, J., and Peles, E. (2014) Long-term maintenance of Na^+ channels at nodes of Ranvier depends on glial contact mediated by gliomedin and NrCAM. *J. Neurosci.* **34,** 5089–5098
7. Eshed, Y., Feinberg, K., Carey, D. J., and Peles, E. (2007) Secreted gliomedin is a perinodal matrix component of peripheral nerves. *J. Cell Biol.* **177,** 551–562
8. Maertens, B., Hopkins, D., Franzke, C. W., Keene, D. R., Bruckner-Tuderman, L., Greenspan, D. S., and Koch, M. (2007) Cleavage and oligomerization of gliomedin, a transmembrane collagen required for node of Ranvier formation. *J. Biol. Chem.* **282,** 10647–10659
9. Labasque, M., Devaux, J. J., Lévêque, C., and Faivre-Sarrailh, C. (2011) Fibronectin type III-like domains of neurofascin-186 protein mediate gliomedin binding and its clustering at the developing nodes of Ranvier. *J. Biol. Chem.* **286,** 42426–42434
10. Desmazieres, A., Zonta, B., Zhang, A., Wu, L. M., Sherman, D. L., and Brophy, P. J. (2014) Differential stability of PNS and CNS nodal complexes when neuronal neurofascin is lost. *J. Neurosci.* **34,** 5083–5088
11. Loria, P. M., Hodgkin, J., and Hobert, O. (2004) A conserved postsynaptic transmembrane protein affecting neuromuscular signaling in *Caenorhabditis elegans*. *J. Neurosci.* **24,** 2191–2201
12. Yokoe, H., and Anholt, R. R. (1993) Molecular cloning of olfactomedin, an extracellular matrix protein specific to olfactory neuroepithelium. *Proc. Natl. Acad. Sci. U.S.A.* **90,** 4655–4659
13. Anholt, R. R. (2014) Olfactomedin proteins: central players in development and disease. *Front. Cell Dev. Biol.* **2,** 6
14. Tomarev, S. I., and Nakaya, N. (2009) Olfactomedin domain-containing proteins: possible mechanisms of action and functions in normal development and pathology. *Mol. Neurobiol.* **40,** 122–138
15. Dismuke, W. M., McKay, B. S., and Stamer, W. D. (2012) Myocilin, a component of a membrane-associated protein complex driven by a homologous Q-SNARE domain. *Biochemistry* **51,** 3606–3613
16. Resch, Z. T., and Fautsch, M. P. (2009) Glaucoma-associated myocilin: a better understanding but much more to learn. *Exp. Eye Res* **88,** 704–712
17. Tamm, E. R. (2002) Myocilin and glaucoma: facts and ideas. *Prog. Retin. Eye Res.* **21,** 395–428
18. Stone, E. M., Fingert, J. H., Alward, W. L., Nguyen, T. D., Polansky, J. R., Sunden, S. L., Nishimura, D., Clark, A. F., Nystuen, A., Nichols, B. E., Mackey, D. A., Ritch, R., Kalenak, J. W., Craven, E. R., and Sheffield, V. C. (1997) Identification of a gene that causes primary open angle glaucoma. *Science* **275,** 668–670
19. Kwon, H. S., Nakaya, N., Abu-Asab, M., Kim, H. S., and Tomarev, S. I. (2014) Myocilin is involved in NgR1/Lingo-1-mediated oligodendrocyte differentiation and myelination of the optic nerve. *J. Neurosci.* **34,** 5539–5551

20. Kwon, H. S., Johnson, T. V., Joe, M. K., Abu-Asab, M., Zhang, J., Chan, C. C., and Tomarev, S. I. (2013) Myocilin mediates myelination in the peripheral nervous system through ErbB2/3 signaling. *J. Biol. Chem.* **288,** 26357–26371
21. Ohlmann, A., Goldwich, A., Flügel-Koch, C., Fuchs, A. V., Schwager, K., and Tamm, E. R. (2003) Secreted glycoprotein myocilin is a component of the myelin sheath in peripheral nerves. *Glia* **43,** 128–140
22. Ricard, C. S., Agapova, O. A., Salvador-Silva, M., Kaufman, P. L., and Hernandez, M. R. (2001) Expression of myocilin/TIGR in normal and glaucomatous primate optic nerves. *Exp. Eye Res.* **73,** 433–447
23. Han, H., and Kursula, P. (2014) Expression, purification, crystallization and preliminary x-ray crystallographic analysis of the extracellular olfactomedin domain of gliomedin. *Acta Crystallogr. F Struct. Biol. Commun.* **70,** 1536–1539
24. Petoukhov, M. V., Franke, D., Shkumatov, A. V., Tria, G., Kikhney, A. G., Gajda, M., Gorba, C., Mertens, H. D., Konarev, P. V., and Svergun, D. I. (2012) New developments in the ATSAS program package for small-angle scattering data analysis. *J. Appl. Crystallogr.* **45,** 342–350
25. Svergun, D. I., Petoukhov, M. V., and Koch, M. H. (2001) Determination of domain structure of proteins from x-ray solution scattering. *Biophys. J.* **80,** 2946–2953
26. Kabsch, W. (1993) Automatic processing of rotation diffraction data from crystals of initially unknown symmetry and cell constants. *J. Appl. Crystallogr.* **26,** 795–800
27. Panjikar, S., Parthasarathy, V., Lamzin, V. S., Weiss, M. S., and Tucker, P. A. (2005) Auto-Rickshaw: an automated crystal structure determination platform as an efficient tool for the validation of an x-ray diffraction experiment. *Acta Crystallogr. D Biol. Crystallogr.* **61,** 449–457
28. Winn, M. D., Ballard, C. C., Cowtan, K. D., Dodson, E. J., Emsley, P., Evans, P. R., Keegan, R. M., Krissinel, E. B., Leslie, A. G., McCoy, A., McNicholas, S. J., Murshudov, G. N., Pannu, N. S., Potterton, E. A., Powell, H. R., Read, R. J., Vagin, A., and Wilson, K. S. (2011) Overview of the CCP4 suite and current developments. *Acta Crystallogr. D Biol. Crystallogr.* **67,** 235–242
29. Sheldrick, G. M. (2010) Experimental phasing with SHELXC/D/E: combining chain tracing with density modification. *Acta Crystallogr. D Biol. Crystallogr.* **66,** 479–485
30. Schneider, T. R., and Sheldrick, G. M. (2002) Substructure solution with SHELXD. *Acta Crystallogr. D Biol. Crystallogr.* **58,** 1772–1779
31. Hao, Q. (2004) ABS: a program to determine absolute configuration and evaluate anomalous scatterer substructure. *J. Appl. Crystallogr.* **37,** 498–499
32. Sheldrick, G. M. (2002) Macromolecular phasing with SHELXE. *Z. Kristallogr.* **217,** 644–650
33. Terwilliger, T. C. (2000) Maximum-likelihood density modification. *Acta Crystallogr. D Biol. Crystallogr.* **56,** 965–972
34. Cowtan, K. (1994) "dm": an automated procedure for phase improvement by density modification. *Joint CCP4 and ESF-EACBM Newsletter on Protein Crystallography*, Vol. 31, pp. 34–38, Daresbury Laboratory, Warrington, United Kingdom
35. Morris, R. J., Zwart, P. H., Cohen, S., Fernandez, F. J., Kakaris, M., Kirillova, O., Vonrhein, C., Perrakis, A., and Lamzin, V. S. (2004) Breaking good resolutions with ARP/wARP. *J. Synchrotron Radiat.* **11,** 56–59
36. Perrakis, A., Morris, R., and Lamzin, V. S. (1999) Automated protein model building combined with iterative structure refinement. *Nat. Struct. Biol.* **6,** 458–463
37. Brünger, A. T., Adams, P. D., Clore, G. M., DeLano, W. L., Gros, P., Grosse-Kunstleve, R. W., Jiang, J. S., Kuszewski, J., Nilges, M., Pannu, N. S., Read, R. J., Rice, L. M., Simonson, T., and Warren, G. L. (1998) Crystallography & NMR system: a new software suite for macromolecular structure determination. *Acta Crystallogr. D Biol. Crystallogr.* **54,** 905–921
38. Murshudov, G. N., Vagin, A. A., and Dodson, E. J. (1997) Refinement of macromolecular structures by the maximum-likelihood method. *Acta Crystallogr. D Biol. Crystallogr.* **53,** 240–255
39. Adams, P. D., Afonine, P. V., Bunkóczi, G., Chen, V. B., Davis, I. W., Echols, N., Headd, J. J., Hung, L. W., Kapral, G. J., Grosse-Kunstleve, R. W., McCoy, A. J., Moriarty, N. W., Oeffner, R., Read, R. J., Richardson, D. C., Richardson, J. S., Terwilliger, T. C., and Zwart, P. H. (2010) PHENIX: a comprehensive Python-based system for macromolecular structure solution. *Acta Crystallogr. D Biol. Crystallogr.* **66,** 213–221
40. Emsley, P., Lohkamp, B., Scott, W. G., and Cowtan, K. (2010) Features and development of Coot. *Acta Crystallogr. D Biol. Crystallogr.* **66,** 486–501
41. Krissinel, E., and Henrick, K. (2004) Secondary-structure matching (SSM), a new tool for fast protein structure alignment in three dimensions. *Acta Crystallogr. D Biol. Crystallogr.* **60,** 2256–2268
42. Margraf, T., Schenk, G., and Torda, A. E. (2009) The SALAMI protein structure search server. *Nucleic Acids Res.* **37,** W480–W484
43. Pettersen, E. F., Goddard, T. D., Huang, C. C., Couch, G. S., Greenblatt, D. M., Meng, E. C., and Ferrin, T. E. (2004) UCSF Chimera–a visualization system for exploratory research and analysis. *J. Comput. Chem.* **25,** 1605–1612
44. Hollup, S. M., Salensminde, G., and Reuter, N. (2005) WEBnm@: a web application for normal mode analyses of proteins. *BMC Bioinformatics* **6,** 52
45. McNicholas, S., Potterton, E., Wilson, K. S., and Noble, M. E. (2011) Presenting your structures: the CCP4mg molecular-graphics software. *Acta Crystallogr. D Biol. Crystallogr.* **67,** 386–394
46. Armon, A., Graur, D., and Ben-Tal, N. (2001) ConSurf: an algorithmic tool for the identification of functional regions in proteins by surface mapping of phylogenetic information. *J. Mol. Biol.* **307,** 447–463
47. Biasini, M., Bienert, S., Waterhouse, A., Arnold, K., Studer, G., Schmidt, T., Kiefer, F., Cassarino, T. G., Bertoni, M., Bordoli, L., and Schwede, T. (2014) SWISS-MODEL: modelling protein tertiary and quaternary structure using evolutionary information. *Nucleic Acids Res.* **42,** W252–W258
48. Fülöp, V., and Jones, D. T. (1999) β Propellers: structural rigidity and functional diversity. *Curr. Opin. Struct. Biol.* **9,** 715–721
49. Chen, C. K., Chan, N. L., and Wang, A. H. (2011) The many blades of the β-propeller proteins: conserved but versatile. *Trends Biochem. Sci.* **36,** 553–561
50. Nayal, M., and Di Cera, E. (1996) Valence screening of water in protein crystals reveals potential Na^+ binding sites. *J. Mol. Biol.* **256,** 228–234
51. Zheng, H., Chordia, M. D., Cooper, D. R., Chruszcz, M., Müller, P., Sheldrick, G. M., and Minor, W. (2014) Validation of metal-binding sites in macromolecular structures with the CheckMyMetal web server. *Nat. Protoc.* **9,** 156–170
52. Donegan, R. K., Hill, S. E., Turnage, K. C., Orwig, S. D., and Lieberman, R. L. (2012) The glaucoma-associated olfactomedin domain of myocilin is a novel calcium binding protein. *J. Biol. Chem.* **287,** 43370–43377
53. Svergun, D., Barberato, C., and Koch, M. H. (1995) CRYSOL–a program to evaluate x-ray solution scattering of biological macromolecules from atomic coordinates. *J. Appl. Crystallogr.* **28,** 768–773
54. Burns, J. N., Turnage, K. C., Walker, C. A., and Lieberman, R. L. (2011) The stability of myocilin olfactomedin domain variants provides new insight into glaucoma as a protein misfolding disorder. *Biochemistry* **50,** 5824–5833
55. Orwig, S. D., and Lieberman, R. L. (2011) Biophysical characterization of the olfactomedin domain of myocilin, an extracellular matrix protein implicated in inherited forms of glaucoma. *PLoS ONE* **6,** e16347
56. Aroca-Aguilar, J. D., Sánchez-Sánchez, F., Ghosh, S., Coca-Prados, M., and Escribano, J. (2005) Myocilin mutations causing glaucoma inhibit the intracellular endoproteolytic cleavage of myocilin between amino acids Arg^{226} and Ile^{227}. *J. Biol. Chem.* **280,** 21043–21051
57. Aroca-Aguilar, J. D., Sánchez-Sánchez, F., Martínez-Redondo, F., Coca-Prados, M., and Escribano, J. (2008) Heterozygous expression of myocilin glaucoma mutants increases secretion of the mutant forms and reduces extracellular processed myocilin. *Mol. Vis.* **14,** 2097–2108
58. Hill, S. E., Donegan, R. K., and Lieberman, R. L. (2014) The glaucoma-associated olfactomedin domain of myocilin forms polymorphic fibrils that are constrained by partial unfolding and peptide sequence. *J. Mol. Biol.* **426,** 921–935
59. Vollrath, D., and Liu, Y. (2006) Temperature sensitive secretion of mutant myocilins. *Exp. Eye Res.* **82,** 1030–1036
60. Yam, G. H., Gaplovska-Kysela, K., Zuber, C., and Roth, J. (2007) Aggregated myocilin induces Russell bodies and causes apoptosis: implications for the pathogenesis of myocilin-caused primary open-angle glaucoma. *Am. J. Pathol.* **170,** 100–109
61. Feinberg, K., Eshed-Eisenbach, Y., Frechter, S., Amor, V., Salomon, D.,

Sabanay, H., Dupree, J. L., Grumet, M., Brophy, P. J., Shrager, P., and Peles, E. (2010) A glial signal consisting of gliomedin and NrCAM clusters axonal Na^+ channels during the formation of nodes of Ranvier. *Neuron* **65,** 490–502

62. Devaux, J. J. (2012) Antibodies to gliomedin cause peripheral demyelinating neuropathy and the dismantling of the nodes of Ranvier. *Am. J. Pathol.* **181,** 1402–1413
63. Devaux, J. J., Odaka, M., and Yuki, N. (2012) Nodal proteins are target antigens in Guillain-Barré syndrome. *J. Peripher. Nerv. Syst.* **17,** 62–71
64. Notturno, F., Di Febo, T., Yuki, N., Fernandez Rodriguez, B. M., Corti, D., Nobile-Orazio, E., Carpo, M., De Lauretis, A., and Uncini, A. (2014) Autoantibodies to neurofascin-186 and gliomedin in multifocal motor neuropathy. *J. Neuroimmunol.* **276,** 207–212
65. Hillier, B. J., and Vacquier, V. D. (2003) Amassin, an olfactomedin protein, mediates the massive intercellular adhesion of sea urchin coelomocytes. *J. Cell Biol.* **160,** 597–604
66. Hillier, B. J., and Vacquier, V. D. (2007) Structural features and functional domains of amassin-1, a cell-binding olfactomedin protein. *Biochem. Cell Biol.* **85,** 552–562
67. Nagy, I., Trexler, M., and Patthy, L. (2003) Expression and characterization of the olfactomedin domain of human myocilin. *Biochem. Biophys. Res. Commun.* **302,** 554–561
68. McDowell, C. M., Luan, T., Zhang, Z., Putliwala, T., Wordinger, R. J., Millar, J. C., John, S. W., Pang, I. H., and Clark, A. F. (2012) Mutant human myocilin induces strain specific differences in ocular hypertension and optic nerve damage in mice. *Exp. Eye Res.* **100,** 65–72
69. Karplus, P. A., and Diederichs, K. (2012) Linking crystallographic model and data quality. *Science* **336,** 1030–1033
70. Davis, I. W., Leaver-Fay, A., Chen, V. B., Block, J. N., Kapral, G. J., Wang, X., Murray, L. W., Arendall, W. B., 3rd, Snoeyink, J., Richardson, J. S., and Richardson, D. C. (2007) MolProbity: all-atom contacts and structure validation for proteins and nucleic acids. *Nucleic Acids Res.* **35,** W375–W383
71. Huang, W. L., Wang, Y. R., Ko, T. P., Chia, C. Y., Huang, K. F., and Wang, A. H. (2010) Crystal structure and functional analysis of the glutaminyl cyclase from *Xanthomonas campestris*. *J. Mol. Biol.* **401,** 374–388
72. Canning, P., Cooper, C. D., Krojer, T., Murray, J. W., Pike, A. C., Chaikuad, A., Keates, T., Thangaratnarajah, C., Hojzan, V., Ayinampudi, V., Marsden, B. D., Gileadi, O., Knapp, S., von Delft, F., and Bullock, A. N. (2013) Structural basis for Cul3 protein assembly with the BTB-Kelch family of E3 ubiquitin ligases. *J. Biol. Chem.* **288,** 7803–7814

The Olfactomedin Domain from Gliomedin Is a β-Propeller with Unique Structural Properties

Huijong Han and Petri Kursula

J. Biol. Chem. 2015, 290:3612-3621.
doi: 10.1074/jbc.M114.627547 originally published online December 17, 2014